The 1998 Mars Global Surveyor Solar Corona Experiment

D. Morabito,[1] S. Shambayati,[1] S. Butman,[1] D. Fort,[2] and S. Finley[2]

The Mars Global Surveyor (MGS) spacecraft, launched on November 7, 1996, carries an experimental space-to-ground telecommunications link at 32 GHz (Ka-band) along with the primary 8.4-GHz (X-band) downlink used for operational MGS project activities. The signals are simultaneously transmitted from a 1.5-m-diameter parabolic antenna on MGS and received by 34-meter beam-waveguide (BWG) antennas located at NASA's Goldstone Deep Space Communications Complex near Barstow, California. Relative signal strength data demonstrating the advantage of Ka-band over X-band as well as details of analysis of the frequency data were presented in previous articles. This article will focus on details of the Ka-band and X-band observations acquired during the May 1998 solar conjunction experiment at solar elongation angles below 3 deg. For the link study, the Ka-band data were recorded open loop using the full spectrum recorder (FSR), and most of the X-band data were obtained from the closed-loop Block V receivers of the operational Deep Space Network. In addition, a few selected passes were conducted where open-loop FSR data were recorded at X-band. Among the solar coronal effects on signal propagation presented will be intensity scintillation and spectral broadening. Also presented are frequency data results acquired using DSS 13's experimental tone tracker.

I. Introduction

The use of 32 GHz (Ka-band) as a telecommunications link frequency is predicted to add about a 5-dB advantage in gain over that of 8.4 GHz (X-band), the primary deep-space telecommunications link frequency in use today. This link advantage was demonstrated by using the signal strength data acquired from the first 2 years of the Mars Global Surveyor (MGS) Ka-band link experiment (MGS/KaBLE-II) as well as by successfully conducting end-to-end telemetry and ranging demonstrations [1–3]. MGS/KaBLE-II also measured frequency residuals, which were in agreement between bands and whose statistics were consistent with expected noise sources [4]. This article will focus on data acquired during the May 1998 solar conjunction of MGS to study the effects of the solar plasma on the received signals.

---

[1] Communications Systems and Research Section.

[2] Antenna Systems and Applications Section.

The research described in this publication was carried out by the Jet Propulsion Laboratory, California Institute of Technology, under a contract with the National Aeronautics and Space Administration.

Deep-space missions, which often fly in the ecliptic (the region of the sky that contains the planets and the Sun), typically encounter solar conjunctions. The communications link between an interplanetary spacecraft and the Earth is affected by the solar corona and solar wind. As the Sun–Earth–probe (SEP) angle becomes small, the signal suffers increased degradation. The effects on the received signal include time delay due to the columnar integrated electron density and phase fluctuations due to the columnar fluctuating electron density, which in turn cause carrier lock problems and telemetry data loss. Signal phase fluctuation effects are most visible as Doppler noise. Both signal amplitude and phase fluctuations also are observable as spectral broadening. These effects are frequency dependent, as time delay scales as $1/f^2$ and phase fluctuation scales as $1/f$. These effects correlate with solar radial distance, heliocentric latitude, and the phase of the solar cycle.

Feria et al. [5] presented a model to study amplitude scintillation effects on telemetry signals at both X-band and Ka-band. Their analytical and simulation results showed that, at an SEP angle of about 1 deg, the X-band telemetry link suffers degradation of more than 8 dB, whereas the Ka-band telemetry link degrades less than 0.2 dB.

Over the past several years, many observations of the degradation of 2.3-GHz (S-band) and X-band downlink signals have been made at small SEP angles. In the case of the Galileo spacecraft at S-band, results of the arraying of tracking data from the 1994 conjunction[3] showed that the solar plasma induced a few tenths of a dB loss at SEP angles between 10 and 15 deg. The loss grew to 0.5 dB at a 5-deg SEP angle and to several dB below a 5-deg SEP angle. The Magellan spacecraft downlink performance allowed telemetry to be tracked down to a 0.6-deg SEP angle at X-band.[4] The Voyager 2 spacecraft solar conjunction in December 1987 probed SEP angles down near 1 deg at X-band [6]. Carrier signal power degraded by about 8 dB at a 1-deg SEP angle and by about 4 dB at a 2-deg SEP angle.

The Near Earth Asteroid Rendezvous (NEAR) spacecraft X-band solar corona experiment found good downlink performance at an SEP angle of 2.3 deg but poor performance at an SEP angle of 1.1 deg at both 1104- and 39.4-b/s bit rates [7]. The poor 39.4-b/s low-rate data were thought to be due to either the longer frame time or scintillation-induced phase noise in the ground receiver carrier tracking loop. The receiver settings were considered to be nonoptimal. By better characterizing the scintillation environment, more optimal receiver settings can be realized. For future missions, the appropriate amount of transmitter power can be implemented to overcome solar conjunction effects and establish a reliable downlink.

The measurement of Doppler frequency during superior conjunctions of planetary spacecraft is an important tool used to remotely probe the solar wind. The Pioneer Venus Orbiter (PVO) underwent seven solar conjunctions between 1979 and 1990, which covered a full solar cycle [8]. The solar wind was probed to within 0.43 AU of the Sun for this study using S-band and X-band data.

This article will focus on the analysis of tracking data acquired during the solar conjunction period of May 1998 as MGS, in orbit around Mars, passed angularly near the Sun as viewed from Earth. The spacecraft and station configurations first will be briefly described, followed by descriptions of models for scintillation and spectral broadening. Finally, the results of the data analysis will be presented.

---

[3] R. Kahn, "Analysis of November/December 1994 Galileo Array Conjunction Data," JPL Interoffice Memorandum 335.1-96-003 (internal document), Jet Propulsion Laboratory, Pasadena, California, February 6, 1996.

[4] J. Webster, "Magellan Spacecraft Performance During Solar Conjunction," JPL Interoffice Memorandum 3395-94-44 (internal document), Jet Propulsion Laboratory, Pasadena, California, August 4, 1994, in *Collected Papers on the Performance of an X-band Signal Near the Sun*, JPL D-15636 (internal document), Jet Propulsion Laboratory, Pasadena California, March 1998.

II. Spacecraft Configuration

The Ka-band downlink signal is derived from a sample of the spacecraft X-band downlink signal, which is upconverted to 32 GHz, amplified, and radiated from a dual-frequency (X-/Ka-band) high-gain antenna (HGA). The X-band link uses a transmit power of 25 W from a traveling-wave tube amplifier (TWTA), while the Ka-band link uses a 1.5-W transmit power output from a solid-state power amplifier (SSPA). The effective isotropic radiated power (EIRP) is about 82 dBm for the X-band link and about 76 dBm for the Ka-band link.

The upconversion is accomplished by first downconverting the X-band sample at 8.42 GHz to a frequency of 8 GHz, which then is multiplied by a X4 multiplier, producing the required 32-GHz Ka-band frequency in the Deep Space Network (DSN) allocation band.

During the first 2 years of the link experiment, the Ka-band downlink frequency was either coherent with the X-band downlink frequency or a hybrid combination of ultra-stable oscillator (USO)- and voltage-controlled oscillator (VCO)-derived frequencies, depending upon the X-band uplink status and the programmed setting of a switch onboard the spacecraft. The Ka-band downlink signal is coherent with the X-band downlink signal when the downconverter is driven by the same frequency source as the X-band signal. During the 1998 solar conjunction, the spacecraft was configured to be coherent in the one-way mode; that is, the Ka-band frequency is a factor of 3.8 times the X-band frequency during one-way periods and a hybrid combination of the X-band USO and VCO during the three-way periods.

MGS utilized an autonomous sequence during the solar conjunction period from 98-120 (year/day of year) to 98-146. The spacecraft sequence continually cycled between 6 hours in a Sun-pointed attitude and 2 hours of Earth-pointing attitude. The spacecraft telecommunications subsystem was reconfigured for each attitude change in an attempt to maintain contact with Earth. During Sun-pointed periods, the spacecraft utilized the low-gain antenna (LGA) and the telecommunications rate was set to 10 b/s. When the spacecraft was Earth pointed, the HGA was utilized and the downlink telemetry rate was 2000 b/s.

III. Ground System Configuration

The ground station used to acquire the Ka-band data is Deep Space Station (DSS) 13, a 34-meter beam-waveguide (BWG) antenna located at NASA's Goldstone Deep Space Communications Complex near Barstow, California. This antenna incorporates a series of mirrors inside beam-waveguide tubes that guide and focus the RF energy onto feed horns on low-noise amplifiers (LNAs) residing in a subterranean pedestal room. A dichroic plate allows simultaneous reception of both X-band and Ka-band signals. The RF signals are amplified by high-electron mobility transistor (HEMT) LNAs and then are downconverted to IF near 300 MHz and transported via optical fiber to a control room where they are input to the receivers.

The experimental tone tracker (ETT) is a digital phase-locked-loop (PLL) receiver that was used to simultaneously track both X-band and Ka-band carrier signals at DSS 13. The analog IF signal input to the ETT is open-loop downconverted to baseband and then digitized. Once a signal is detected, the ETT's digital PLLs extract estimates of the carrier signal-to-noise ratio (SNR), P_c/N_o, in a 1-Hz bandwidth as well as the phase and frequency at baseband.

During the May 1998 solar conjunction of Mars and MGS, the ETT at DSS 13 acquired dual-frequency X-band and Ka-band carrier data using equivalent tracking loop settings. The carrier signal level estimates (P_c/N_o) of Ka-band were compared with those of X-band. A significant advantage of Ka-band relative to X-band was measured, showing values as much as 30-dB higher at small SEP angles. The Ka-band signal was tracked more easily than the X-band signal (when spacecraft pointing and weather cooperated), and

this was most dramatically demonstrated during the tracking pass on 98-128 when the Ka-band signal was tracked nearly continuously for over an hour while the ETT managed to lock onto the X-band signal for only a few seconds.

Throughout the MGS Ka-/X-band data acquisition period from December 1996 to December 1998, the ETT measured P_c/N_o estimates that were within 0.5 dB of predicts. The ETT also produced frequency estimates that were of excellent quality and whose statistics were consistent with those of the expected noise sources at the appropriate time scales [4].

However, because of known deficiencies of the ETT in responding to high signal dynamics and nonoptimum receiver settings, the P_c/N_o estimates for X-band (and possibly Ka-band) at small SEP angles were degraded as compared with measurements that could be made from more sophisticated receivers. The high dynamics present during small SEP angles are caused by scintillations induced by the solar plasma on the link. Fade durations can last several milliseconds, which translates to several update intervals in the PLL. The failure to adapt to these large fades causes difficulties in tracking or reduction in reported P_c/N_o. Thus, at least at X-band, the ETT performance was found to be worse than the Block V receiver (BVR) performance during the solar conjunction. At a 3-deg SEP angle, the ETT X-band P_c/N_o was about 3 to 5 dB below the predicted value, while the BVR measurements were within 1 dB of the predicts.

Closed-loop BVR data from the 34-m antennas of the operational DSN tracking network were used for much of the X-band data in the study described in this article. These data were acquired using a loop bandwidth of 3 Hz for much of the solar conjunction period. The data were extracted from monitor data archived by the Radio Science Group. A few select passes of open-loop X-band data were acquired during the solar conjunction using the full-spectrum recorder (FSR) at Signal Processing Center (SPC) 10.

Open-loop FSR data from DSS 13 were used for much of the Ka-band results presented in this article. The FSR translates the input IF band (265 to 375 MHz) down to 9 to 119 MHz by filtering and mixing with a 256-MHz local oscillator (LO) signal. The shifted IF band is sampled at 256 Msamples/s with 8-bit resolution. A variable attenuator in front of the sampler can be set to optimize the use of the 8-bit resolution (in order to minimize saturation and digital noise). The resulting digital data stream then is mixed with quadrature LOs and filtered to produce a complex baseband channel of -8 to $+8$ MHz, with a resolution of 8 bits for both the real and imaginary parts. The frequency of the LO is user-specified in steps of 1 MHz. For the experiments described in this article, the baseband data are phase rotated by a phase model generated by predicts in order to bring the spacecraft carrier signal frequency to a nominal 0 Hz. The data acquired during the May 1998 solar conjunction experiment (small SEP angles) thus were filtered and decimated to produce complex data at 5000 samples per second, while the October 1999 experiment data (a high SEP-angle pass used to define signal line width in flight) were sampled at 6400 samples per second.

IV. Solar Model

A. Intensity Scintillations

The scintillation index, m, is defined as the ratio of the rms intensity fluctuation relative to the mean intensity, and it characterizes the strength of the small-scale density fluctuations ($\tilde{<}$ Fresnel zone size $= \sqrt{\lambda z}$, where z is the effective scattering screen distance) of the solar plasma charged particles. For weak scattering, the scintillation index, m, is given by the following equation [9]:

$$m = 2k^{7/12}(a_1 R)^{1/2} \left(\frac{L_1 L_2}{L}\right)^{5/12} c_{no} \tag{1}$$

where

$k =$ the radio wave number $(2\pi/\lambda)$

$a_1 = 0.85$

$R =$ the distance between the Earth–spacecraft signal's closest approach and the Sun

$L_1 =$ the distance from Earth to the point of the signal's closest approach to the Sun

$L_2 =$ the distance from the point of the signal's closest approach to the Sun to the spacecraft

$L = L_1 + L_2$

$c_{no} =$ the structure constant that characterizes the magnitude of the fluctuations

The structure constant is a function of the rms electron density fluctuation [9], σ_{ne}:

$$c_{no} = \frac{\sigma_{ne} k^{-2} L_o^{-1/3}}{4.1 \times 10^{13}}$$

where L_o is the outer scale of turbulence. Note that the structure constant is proportional to λ^2, so that scintillation effects will be worse for the higher wavelength (lower frequency) X-band than for Ka-band.

From the above, we thus find that the ratio of the scintillation indices at MGS's Ka-band and X-band frequencies is

$$\frac{m_{Ka}}{m_X} = \left(\frac{\lambda_{Ka}}{\lambda_X}\right)^{17/12} = 0.15 \tag{2}$$

where we have made use of the relation $c_{no} \sim \lambda^2$. Since $m_{Ka}/m_X = 0.15$ in the realm of weak scattering, the relative fluctuations for Ka-band should be only 15 percent of those of the X-band signal.

In the realm of strong scattering, intensity scintillation will saturate with increasing turbulence. Thus, below the SEP angle at which strong scattering begins, the scintillation index reaches a value of unity and for a point source there will not be any further increase as the SEP angle decreases. Thus, for strong scattering, $m = 1$, and the time scale of the scintillations becomes shorter. Given that m_X starts saturating at about a 1.25-deg SEP angle, the expected saturation of m_{Ka} should occur near an SEP angle of 0.67 deg. The measured scintillation index may differ from that of the quiet background, depending upon solar activity (flares, coronal mass ejections (CMEs), corotating structures, etc.) and the effects of any nonoptimal receiver settings.

B. Spectral Broadening

Spectral broadening is dependent on both electron density fluctuations and solar wind velocity, whereas the scintillation index depends on the electron density fluctuations only. Spectral broadening is useful only when the observations are conducted close enough to the Sun such that the broadening exceeds the line width of the oscillator. Oscillator line widths are typically <0.02 Hz for USOs and <3 Hz for auxiliary oscillators at X-band.[5] Spectral broadening responds mostly to smaller scales and is similar to intensity scintillations, which respond only to small-scale sizes due to Fresnel filtering.

The bandwidth, B, of the received signal due to spectral broadening for both weak and strong scattering is given by [9]

[5] A. Makovsky, personal communication, Communications Systems and Research Section, Jet Propulsion Laboratory, Pasadena, California, July 12, 2000.

$$B = 0.542k^{6/5}(a_1 R)^{3/5} c_{no}^{6/5} v \tag{3}$$

where v is the solar wind velocity component that lies transverse to the line of sight and the other parameters are as given in Eq. (1).

Based on Eq. (3), the dependence of the broadening with wavelength is seen to be

$$B \sim \lambda^{6/5} \tag{4}$$

Thus, X-band should show a factor of about five times more spectral broadening than Ka-band for a simultaneous observation at the same SEP angle, assuming both exceed the line width of the oscillator.

V. Results

The prime MGS received signal data for the solar conjunction experiment were acquired from the operational BVRs for X-band and from the DSS-13 FSR and ETT for Ka-band, both during periods when the MGS HGA was Earth pointed. The operational DSN 34-m antenna tracking passes between 98-121 07:00 UTC and 98-142 00:00 UTC provided carrier P_c/N_o data from the BVR carrier tracking loops. Due to power constraints, the Ka-band equipment onboard the spacecraft was turned on during those times of the day when the HGA was Earth-pointed. Thus, Ka-band passes at DSS 13 were scheduled only for 2-hour segments between 14:00 and 16:00 UTC and between 22:00 and 24:00 UTC. However, problems with the spacecraft star tracker caused degraded pointing during the conjunction, and there was bad weather during several of the ingress passes. These effects, as well as known problems with the spacecraft KaBLE equipment [1], significantly degraded the received Ka-band signal level.

This section describes the results of the analysis performed on the X-band and Ka-band data acquired from MGS. Between May 1 and May 24, 1998, 35 2-hour tracks were scheduled at DSS 13. The SEP angle ranged from 2.7 deg on 98-121 (May 1) to 0.09 deg on 98-132 (May 12) to 2.4 deg on 98-142 (May 22). On May 12, the spacecraft (and Mars) went behind the disk of the Sun (0.09 deg from the disk center). During those passes in which the spacecraft was behind the disk of the Sun, DSS 13 did not point at the Sun or actively acquire tracking data. The data acquisition occurred during a period when solar activity ranged from a near-minimum to a moderate level. Figure 1 displays this period of the MGS solar conjunction against a plot of sunspot number,[6] which is an indicator of activity during the solar cycle.

The following measurement results will be discussed: system operating noise temperature, T_{op}, increase; X-band P_c/N_o; Ka-band P_c/N_o; X-band open-loop data; Ka-band open-loop data; and X-/Ka-band frequency difference data.

A. System Operating Noise Temperature Increase Due to Solar Noise

The effect of solar radiation on T_{op} as measured by the total power radiometer (TPR) at DSS 13 for both X-band and Ka-band is shown in Fig. 2(a) as a function of SEP angle. These measurements represent increases over the background average temperature at a 3-deg SEP angle (45 K for X-band and 79 K for Ka-band). The actual temperatures were averaged over each pass, so the value may be higher or lower depending upon elevation angle range over the pass. The Ka-band temperature increase to T_{op} due to solar noise normally should be less than that at X-band. However, the increased Ka-band temperature increases over X-band during ingress (at an SEP angle >0.6 deg) is indicative of cloudy and rainy weather during that period (Ka-band is more susceptible to turbulent weather effects), while the

[6] Plot created by U.S. Department of Commerce, National Oceanic and Atmospheric Administration (NOAA), Space Environment Center (web site at http://sec.noaa.gov).

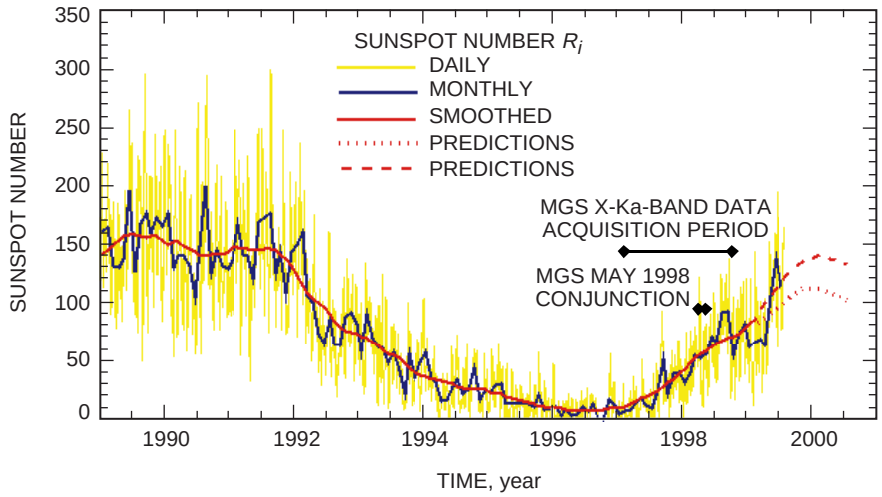

Fig. 1. Sunspot number versus year for both monthly and smoothed values. Sunspot number is one indicator of solar activity over a solar cycle.

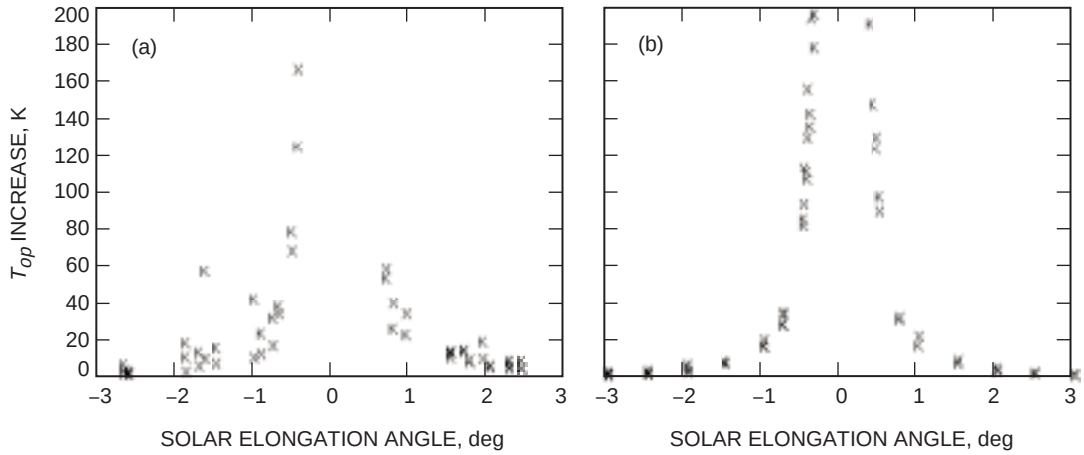

Fig. 2. Measured temperature increase versus SEP angle (a) due to solar corona effects and (b) taken during a planning session in 1996. (X = X-band and K = Ka-band.)

egress data points are comparable. At SEP angles well within 0.6 deg, the solar noise contribution to T_{op} was much higher. Thus, the X-band T_{op} was measured to be higher than that of Ka-band. The T_{op} was measured on day 98-132 to be about 10,500 K at X-band and 5,860 K at Ka-band at an SEP angle of 0.22 deg while on the disk of the Sun [these data points are outside the scale of Fig. 2(a)]. During passes with SEP angles within 0.3 deg, the ground antenna did not actively point at the Sun and track. The measured temperature increases of Fig. 2(a) can be compared with those of earlier cold sky T_{op} data taken during a test session in early 1996 as part of the planning activities for the solar conjunction experiment at DSS 13 (see Fig. 2(b) and note that some of the X-band data points are off the scale). It should be stressed that the planning session data [Fig. 2(b)] were acquired within an hour on a single day during clear weather, while the solar conjunction measurements [Fig. 2(a)] were acquired over a 1-month period over varying weather conditions and different elevation angle spans. The X-band measurements were found to be consistent with similar measurements using a 34-m HEF antenna [10].

B. X-Band BVR Carrier Signal-to-Noise Density, P_c/N_o

The X-band data used here were acquired using the BVRs at the operational 34-m antennas while tracking the MGS spacecraft with the HGA as the signal source. Table 1 summarizes the 34-m DSN BVR

tracking passes used in the X-band study. Listed in Table 1 are the pass identification (ID) (year/day of year); the start and end times of the data analyzed; the DSS station ID; the SEP angle; the average P_c/N_o in dB-Hz; its standard deviations in dB; the scintillation index, m; the average Doppler noise, Hz; and the number of data points averaged. The data points were spaced about 5 to 6 seconds apart.

Table 1. X-band summary from the DSN 34-m antennas using the BVR.

Pass ID	Start, h:min:s	End, h:min:s	DSS	SEP angle, deg	P_c/N_o, dB-Hz	$-\sigma$	$+\sigma$	m	σ_f, Hz	Number of data points
98-121	07:00:00	07:48:00	65	2.79	44.07	0.72	0.61	0.15	0.11	501
98-121	15:00:00	15:30:00	65	2.71	44.79	0.65	0.56	0.14	0.04	310
98-121	23:00:00	24:00:00	45	2.63	43.74	0.74	0.63	0.16	0.35	619
98-122	07:10:00	07:33:00	65	2.55	44.00	0.74	0.63	0.16	0.05	245
98-122	14:15:00	16:00:00	15	2.47	43.35	0.96	0.78	0.20	0.17	1099
98-122	22:20:00	22:38:00	15	2.40	44.34	0.88	0.73	0.18	0.05	186
98-123	07:45:00	08:00:00	65	2.31	43.89	1.27	0.98	0.25	0.15	155
98-123	14:15:00	16:00:00	65	2.23	43.71	1.65	1.19	0.32	0.19	1090
98-123	23:23:00	23:52:00	15	2.15	43.82	1.14	0.90	0.23	0.07	308
98-124	15:35:00	16:00:00	15	1.99	42.83	1.76	1.25	0.33	0.22	249
98-124	22:30:00	23:25:00	15	1.91	43.38	2.10	1.41	0.38	0.82	457
98-125	14:00:00	16:00:00	15	1.75	42.07	3.26	1.84	0.53	0.17	993
98-125	23:15:00	24:00:00	45	1.67	42.32	2.90	1.72	0.49	0.08	472
98-126	07:10:00	08:00:00	65	1.59	40.74	5.84	2.40	0.74	0.27	552
98-126	15:00:00	16:00:00	65	1.51	42.46	6.38	2.48	0.77	—	583
98-127	15:00:00	16:00:00	15	1.26	39.46	6.91	2.54	0.80	0.98	623
98-127	22:40:00	24:00:00	15	1.19	39.38	6.91	3.43	1.20	0.66	796
98-128	07:30:00	08:30:00	65	1.09	37.57	14.84	3.08	1.03	0.28	322
98-128	14:30:00	15:50:00	65	1.02	40.65	4.69	2.20	0.66	0.60	911
98-129	06:40:00	08:30:00	65	0.85	35.80	18.13	3.04	1.02	0.63	862
98-130	06:00:00	07:00:00	54	0.63	17.36	13.04	3.12	1.05	0.37	247
98-135	22:00:00	24:00:00	15	0.77	35.81	13.80	2.92	0.96	0.27	1238
98-136	06:00:00	08:00:00	65	0.85	35.04	16.74	3.06	1.02	0.27	1210
98-136	14:00:00	16:30:00	15	0.94	37.21	13.62	3.10	1.04	0.28	1254
98-136	23:00:00	24:00:00	15	1.01	40.82	5.53	2.36	0.72	1.12	689
98-138	06:00:00	08:00:00	65	1.34	41.49	5.12	2.28	0.69	0.37	1121
98-138	15:00:00	15:50:00	65	1.42	42.76	1.83	1.28	0.34	0.12	545
98-138	22:40:00	24:00:00	15	1.50	42.88	1.60	1.17	0.31	0.11	927
98-139	06:30:00	07:30:00	65	1.58	42.55	1.51	1.12	0.29	0.64	595
98-139	22:30:00	24:00:00	45	1.75	35.86	5.65	2.37	0.73	0.31	923
98-140	06:30:00	07:30:00	65	1.83	37.15	5.16	2.29	0.70	0.09	596
98-140	15:00:00	15:50:00	65	1.91	38.96	5.02	2.27	0.68	0.16	526
98-141	06:30:00	07:30:00	65	2.08	38.89	1.98	1.35	0.37	0.13	463
98-141	14:40:00	16:00:00	65	2.16	43.07	1.87	1.30	0.35	0.19	814
98-141	23:00:00	24:00:00	45	2.24	43.48	1.13	0.89	0.23	0.41	1292

The average P_c/N_o as well as its standard deviation versus SEP angle for each tracking pass are displayed in Fig. 3. Near a ±3-deg SEP angle, the measured values agree well with the 45 dB-Hz predicted value expected without solar corona effects. The lower P_c/N_o for the egress passes is attributed to degraded HGA pointing, which occurred due to an ambiguity in the spacecraft's star map. This problem was corrected after conjunction when the Project was able to command the spacecraft.

Displayed in Fig. 4 is the scintillation index, m, which is defined as the ratio of the standard deviation to the mean of the received P_c/N_o measurements versus SEP angle.[7] It is a measure of the degree of amplitude scintillation on the link when solar effects dominate. The inset SOHO/LASCO[8] image for ingress shows Mars/MGS traversing through a region of lower density and less turbulence, while the scintillation index shows a smooth signature with SEP angle. In contrast, the egress signature was noisier as Mars/MGS was traversing a series of coronal streamers, as displayed in the inset LASCO image for a 2-deg SEP angle at egress. The bumpy structure of the scintillation index during egress is due to increased and decreased scintillation suffered by the signal as the spacecraft goes behind and comes out in between streamers. The group of three data points in Fig. 4 clustered between a 1.75- and a 1.91-deg SEP angle have elevated scintillation indices of 0.73, 0.70 and 0.68, respectively. The inset LASCO image taken at a 2-deg SEP angle at egress shows Mars sitting on a streamer. The group of three data points in Fig. 4 clustered between 2.08- to 2.24-deg SEP angles have reduced scintillation indices of 0.37, 0.35 and 0.23, respectively. Another LASCO image (not shown here) taken concurrently with one of these three passes shows Mars "sitting" in a "quiet" region.

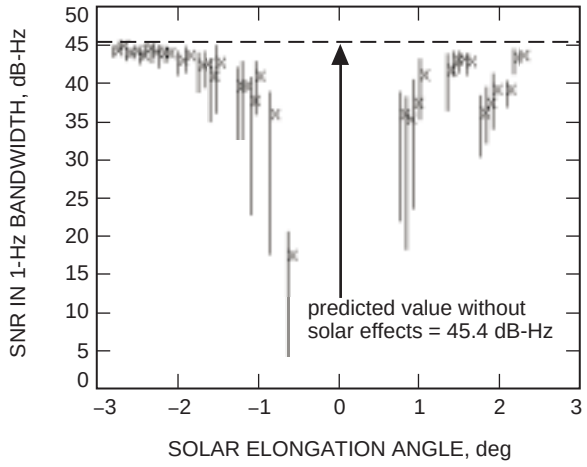

Fig. 3. Averaged X-band P_c/N_o versus SEP angle acquired from the BVR at the 34-m stations.

[7] The Solar Heliospheric Observatory/Large Angle and Spectrometric Coronograph (SOHO/LASCO) data used in the figure were produced by a consortium of the Naval Research Laboratory (USA), the Max-Planck-Institut fuer Aeronomie (Germany), the Laboratoire d'Astronomie (France), and the University of Birmingham (UK). SOHO is a project of international cooperation between the European Space Agency (ESA) and NASA.

[8] The LASCO instrument is one of 11 instruments included on the joint NASA/ESA SOHO spacecraft. The LASCO instrument is a set of three coronagraphs (C1, C2, and C3) that image the solar corona from 1.1 to 32 solar radii ($1Ro = 700,000$ km). A coronagraph is an instrument that is designed to block out light coming from the solar disk in order to image the corona region around the Sun. The C2 telescope and C3 telescope images taken during the period of the MGS solar conjunction were examined. These images proved easy to interpret as Mars typically shows up clearly as a bright spot with an optical artifact (line) and is indicative of the approximate location of the MGS spacecraft.

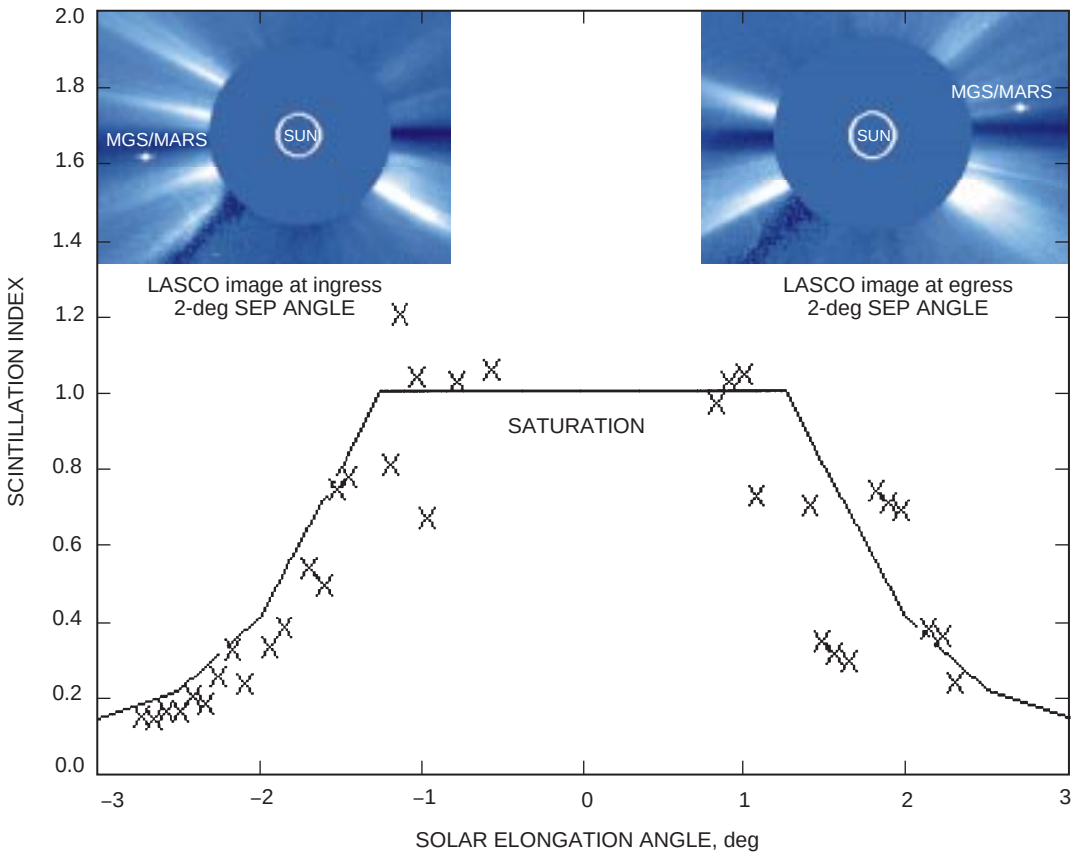

Fig. 4. Measured X-band scintillation index versus SEP angle as determined from $P_c\,/N_o$ acquired from the BVR at the 34-m stations. The solid line depicts the predicted model discussed in the text.

The signature of the scintillation index with SEP angle values is consistent with what is known about the coronal effects on an X-band link.[9] The larger values of scintillation index around 1 and as high as 1.2 are within the realm of expected behavior, including an overshoot effect seen by other investigators and predicted theoretically.[10] Also displayed in Fig. 4 is the solid curve representing the scintillation index using a model developed for a solar probe study.[11] The measured scintillation indices in Table 1 and Fig. 4 for the ingress X-band BVR data appear to be in reasonable agreement with the model. The observed behavior of the measurements during periods when the source was traversing through lower-density, lower-turbulence regions (dark regions on the LASCO images) is expected to lie below the model. The model was derived from spacecraft data acquired over many years primarily in the ecliptic plane, which consists predominately of high-density, high-turbulence regions (bright regions on the LASCO images). However, agreement normally is not expected due to solar conditions (flares, CMEs, etc.). Within this solar conjunction, the scintillation-index signatures for egress and ingress at the same SEP angle differ (see Fig. 4). The ingress scintillation-index measurements follow a reasonably smooth signature with

[9] J. Armstrong and R. Woo, personal communication, Communications Ground Systems Section, Jet Propulsion Laboratory, Pasadena, California, October 13, 1999.

[10] M. Marians, "Theory of Scintillations Due to Propagation Through a Turbulent Medium," Ph.D. dissertation in Applied Physics, University of California, San Diego, 1975.

[11] M. Koerner, "Telemetry and Command Degradation Caused by the RF Signals Amplitude Scintillations Produced by the Near Sun Plasma During the Period Near VRM Superior Conjunction," JPL Interoffice Memorandum 3392-84-64 (internal document), Jet Propulsion Laboratory, Pasadena, California, May 21, 1984, in *Collected Papers on the Performance of an X-band Signal Near the Sun*, JPL D-15636 (internal document), Jet Propulsion Laboratory, Pasadena California, March 1998.

the SEP angle just below the model prior to saturation. The egress scintillation-index measurements lie above and below the model curve as the source traverses on and between streamers.

C. Ka-Band ETT and FSR Signal-to-Noise Density

The Ka-band closed-loop data were acquired using the ETT at DSS 13, as summarized in Table 2. The Ka-band open-loop data from the FSR were processed by a software PLL to produce estimates of relative SNR. The ETT results are documented in Table 2, which lists the pass ID (year/day of year, designation a or b); the SEP angle; the start and end times of the data analyzed; the number of seconds of data used; the average P_c/N_o in dB-Hz; the ratio of scatter to mean intensity (in linear units); the average T_{op} measured over the pass; and comments.

Since the ETT receiver settings were considered nonoptimum and there were passes of turbulent weather, the relative rms scatter over mean intensity in Table 2 should not be considered the scintillation index due to charged particles. Given that Ka-band is susceptible to weather effects, the measured fluctuations may be dominated by the atmosphere at certain times, as is the case with the rainy weather passes. However, there is a tendency for this measurement to take on larger values close in to the Sun.

The FSR at DSS 13 was used to routinely record the Ka-band data during the DSS 13 experiments. The data were recorded at 5000 samples per second and recorded on EXABYTE tapes. The tapes then were post-processed by a variety of software tools to condition and display the data. The FSR open-loop samples were processed by a software PLL to produce estimates of relative SNR. Presented in Figs. 5(a) and 5(b) are the relative signal power versus time for passes 98-125a (SEP = 1.75 deg) and 98-128b (SEP = 0.94 deg), respectively. Note the significantly larger fluctuations for the pass with the smaller SEP angle, pass 98-128b [Fig. 5(b)], relative to that of pass 98-125a [Fig. 5(a)]. Measured values of the relative fluctuations from the PLL output estimates of relative signal power are significantly higher for pass 98-128b (0.37) than for pass 98-125a (0.16).

D. X-Band FSR Data Analysis Results

During selected passes, X-band open-loop FSR data were recorded at the rate of 5000 samples per second. Open-loop X-band FSR data from the passes listed in Table 3 were processed.

The open-loop FSR data were processed using a software PLL. Examples of the effects of loop bandwidth settings on relative signal strength are shown in Figs. 6(a) and 6(b) for pass 98-135. During this pass, the SEP angle was at 0.76 deg. Figure 6(a) displays the relative signal strength for a loop bandwidth setting of 30 Hz, while Fig. 6(b) displays relative signal strength for a loop bandwidth setting of 3 Hz. The measured fluctuation changed very little from 0.76 at B_L = 30 Hz to 0.77 at B_L = 3 Hz, while the average signal level degraded about 2.7 dB by going from B_L = 30 Hz to 3 Hz. By comparison, the measured m from BVR data was found to be about 0.96 for another pass conducted on 98-135 (see Table 1).

The measured scintillation index thus could depend upon receiver type and receiver settings. A too narrow PLL loop bandwidth may not pass all of the fluctuations (it cuts off the higher frequency fluctuation) and thus results in the lower saturated power level. It is difficult to predict the effect on the scintillation index without careful analysis. However, in order to get the correct estimate of m one would achieve using a perfect receiver, one should widen the loop bandwidth until the measured scintillation index becomes stable. Given that the broadened spectrum for this pass is 2.2 Hz (see below), the widening of the loop bandwidth from 3 Hz to 30 Hz did not cause the measured fluctuations using the PLL or the FSR data to significantly change. The fact that the level of these fluctuations (0.77) lies below the BVR-data-derived estimate (0.96) could be attributed to filtering effects in the PLL algorithm.

Fast Fourier transforms (FFTs) were performed on the open-loop FSR samples to produce spectral power density plots in order to measure spectral broadening due to solar effects or the oscillator. The

open-loop samples first were rotated to remove residual unmodeled Doppler and any long period trends due to unmodeled spacecraft motion.

Table 2. Ka-band pass summary from DSS-13 ETT one-way passes.

Pass ID	SEP angle, deg	Start, h:min:s	End, h:min:s	Number of seconds	P_c/N_o, dB-hz	σ/μ, P_c/N_o	T_{op}, K	Comments
98-121a	2.71	15:51:00	16:00:14	555	24.3	0.090	81.2	Clear weather. No monopulse tracking.
98-121b	2.64	22:06:40	22:37:42	1863	23.1	0.237	78.7	—
98-124a	1.92	23:52:10	24:00:29	500	23.4	0.134	96.0	Cloudy weather.
98-125a	1.75	15:15:14	15:36:03	1248	17.4	0.389	125.7	High relative humidity.
98-125b	1.68	22:07:21	23:59:40	4804	16.5	0.611	135.3	Rain.
98-126a	1.52	15:58:00	16:00:35	156	22.0	0.121	94.0	Overcast.
98-126b	1.43	—	—	—	—	—	—	HGA off Earth point.
98-128a	1.03	14:07:04	14:07:51	46	15.3	0.166	120.1	Clear weather.
98-128b	0.96	22:06:32	23:21:16	3913	20.0	0.435	102.2	Clear weather.
98-129a	0.78	—	—	—	—	—	110.0	Cloudy weather; no signal.
98-129b	0.70	—	—	—	—	—	116.4	Partly cloudy; no signal.
98-130a	0.54	—	—	—	—	—	156.5	Clear but windy; X-band in and out of lock; no Ka-band lock.
98-130b	0.46	—	—	—	—	—	202.8	Clear and windy. No signal detected.
98-131a	0.30	—	—	—	—	—	535.0	Clear. No signal detected.
98-131b	0.22	—	—	—	—	—	—	Clear and windy; no signal detected.
98-132a	0.07	—	—	—	—	—	—	MGS behind sun. Did not track.
98-132b	0.05	—	—	—	—	—	—	MGS behind sun. Did not track.
98-134a	0.44	—	—	—	—	—	—	40% puffy white clouds in sky.
98-135a	0.68	—	—	—	—	—	131.6	Clear; no signal.
98-135b	0.76	22:07:03	23:59:49	644	19.8	0.456	104.3	Clear.
98-136a	0.92	15:29:47	15:54:00	652	21.5	0.356	99.9	Light clouds.
98-136b	1.01	22:07:07	24:00:09	1072	12.5	0.484	—	Clear with some high clouds. No TPR data.
98-138a	1.49	23:55:51	24:01:16	326	23.3	0.159	91.2	Clear.
98-139a	1.67	—	—	—	—	—	89.0	Light clouds. HGA 10 deg off point.
98-139b	1.74	22:10:11	22:13:15	185	20.2	0.305	86.2	Clear. HGA off Earth point.
98-140a	1.90	14:08:11	14:13:20	219	18.6	0.328	97.2	Clear. HGA off Earth point.
98-140b	1.99	22:07:31	22:13:49	359	21.4	0.502	83.6	Partly cloudy. HGA off Earth point.
98-141a	2.24	23:52:01	24:01:31	571	23.1	0.137	86.8	Clear.
98-142a	2.40	15:52:41	16:01:32	532	23.4	0.141	82.2	Clear. HGA off Earth point. TPR problems.

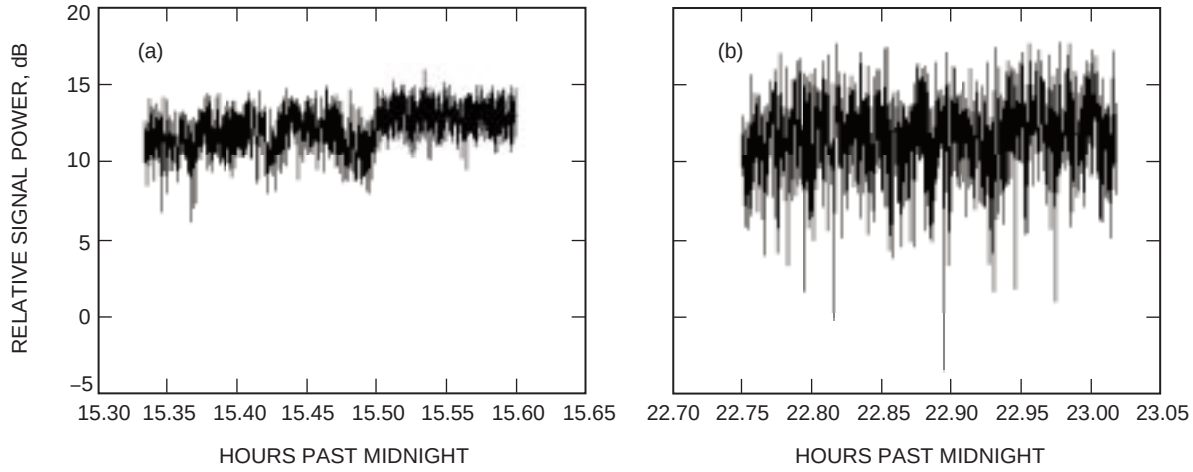

Fig. 5. Measured Ka-band relative signal power estimated from a software PLL using FSR open-loop data recorded at DSS 13 for passes (a) 98-125a from 15:20 to 15:36 UTC at a 1.75-deg SEP angle and (b) 98-128b from 22:45 to 23:01 UTC at a 0.94-deg SEP angle.

Table 3. Open-loop X-band FSR data.

Start time	End time	Station	SEP angle, deg
98-127 23:00	98-127 23:30	DSS 15	1.2
98-127 22:30	98-127 23:50	DSS 45	1.2
98-135 22:06	98-135 22:27	DSS 13	0.76

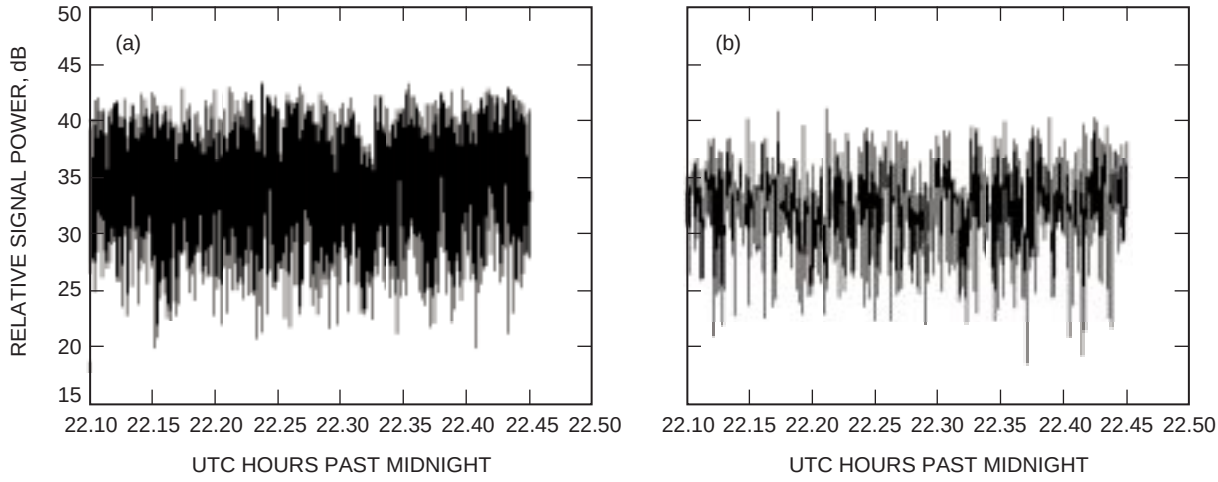

Fig. 6. Relative signal strength versus time in hours UTC for pass 98-135 DSS-13 X-band FSR data processed through a PLL program with (a) B_L = 30 Hz and (b) B_L = 3 Hz.

Figures 7(a) and 7(b) display one-way X-band spectral plots for SEP angles of 0.76 deg for pass 98-135 conducted at DSS 13 and 63 deg for pass 99-303 conducted at DSS 43, respectively. The 99-303 data were acquired as part of a doubly differenced range (DDR) experiment and are used here to define the measured line width in flight at the large 63-deg SEP angle. The measured 2.2-Hz bandwidth for pass 98-135 is thus attributed to spectral broadening due to charged particles at the low 0.76-deg SEP angle and its magnitude is consistent with Viking X-band measurements of 3 to 4 Hz [11] acquired at approximately the same 0.76-deg SEP angle, which corresponds to about 3 solar radii.

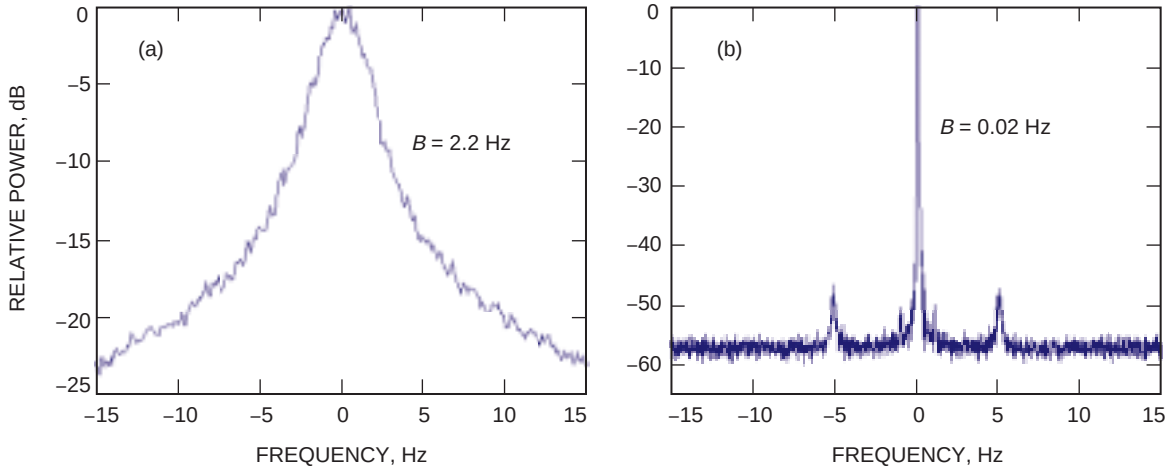

Fig. 7. X-band FFT spectrum plots for passes (a) 98-135, DSS 13, SEP = 0.76 deg, 5000 samples/s, 50,000 samples/FFT, 120 averages, 22:06–22:27 UTC (one way) and (b) 99-303, DSS 43, SEP = 63 deg, 6400 samples/s, 512,000 samples/FFT, 25 averages, 01:05–01:39 UTC (one way) (used as the signal line width reference at high SEP angles).

E. Ka-Band FSR Data Analysis Results

The FSR open-loop samples recorded at DSS 13 also were processed to produce spectral plots. Figures 8(a) through 8(c) display Ka-band spectral plots for SEP angles of 0.94 deg on 98-128 (one-way), 1.75 deg on 98-125 (one-way), and 2.4 deg on 98-142 (three-way with a DSS-15 X-band uplink), respectively. The measured spectral bandwidth of 0.43 Hz for pass 98-128, shown in Fig. 8(a), apparently is due to charged-particle broadening as it is in reasonable agreement with similar results at S-band and X-band [9] at comparable SEP angles [after correcting for known frequency dependence using Eq. (4)]. The spectral bandwidth of about 0.04 Hz for pass 98-125 [Fig. 8(b)] is also consistent with these previous measurements [9] at comparable SEP angles.

The enhanced broadening of the three-way pass on 98-142 [Fig. 8(c)] is primarily attributed to the phase fluctuations on the X-band uplink, which then is multiplied by the 3.8 Ka-/X-band transponder frequency ratio. This contribution is expected to be significantly larger than the additional fluctuations impressed on the Ka-band downlink. Three-way spectra such as those of Fig. 8(c) are more difficult to interpret and have not yet been successfully modeled. The received downlink signal is the result of phase fluctuations on both the uplink and downlink and of amplitude scintillations on the downlink only.

F. Difference Frequency Data

The ETT produced phase and frequency data for passes conducted between January 1997 and December 1998, including the solar conjunction period in May 1998. The estimates of received baseband phase at 1-s sampled time tags from the station-generated ETT data files were converted to received sky frequency estimates using techniques documented in [12]. Frequency residuals for the individual bands were computed by removing a model frequency (including Doppler) from each observable frequency. A

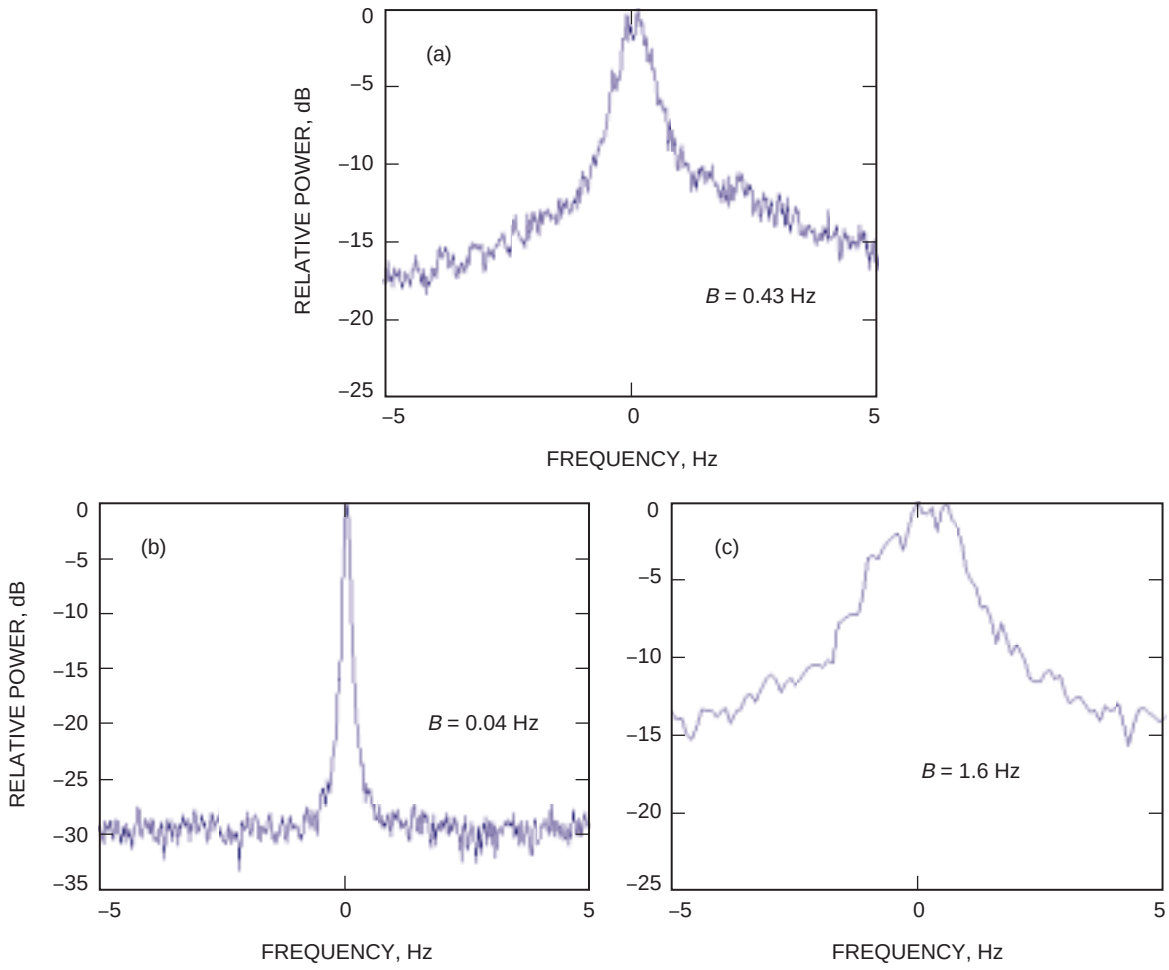

Fig. 8. Ka-band FFT spectrum plots from data recorded at DSS 13 for passes (a) 98-128b, SEP = 0.94 deg, 5000 samples/s, 200,000 samples/FFT, 100 averages, 22:40–23:47 UTC (one way) (b) 98-125a, SEP = 1.75 deg, 5000 samples/s, 200,000 samples/FFT, 24 averages, 15:20–15:36 UTC (one way) and (c) 99-142a, SEP = 2.4 deg, 5000 samples/s, 50,000 samples/FFT, 100 averages, 15:07–15:24 UTC (three-way/DSS-15 uplink).

simple troposphere correction was applied to the data. The model frequency was estimated from MGS Navigation Team trajectory files. Detailed results of the frequency analysis were reported previously in [1] and [4].

For passes when Ka-band is coherent with X-band, the received downlink Ka-band frequency is an exact factor of 3.8 times the X-band received frequency. By taking frequency differences across identical time tags of the form $f_x - f_{Ka}/3.8$, all nondispersive error contributions, including unmodeled dynamic spacecraft motion, USO aging, and troposphere, cancel out in the resulting residuals. The remaining noise sources include thermal noise (significant at small time scales) and charged particles (which dominate at higher time scales). The difference frequencies are effectively a measure of the charged-particle effect on the X-band link since the effect at Ka-band is significantly smaller (by the ratio of the frequencies squared).

The Allan deviations of the difference data type ($f_x - f_{Ka}/3.8$) were estimated. Allan deviation results for time intervals of 1, 10, 100, and 1000 s were presented in [1]. The 100-s and 1000-s Allan deviations are displayed in Figs. 9(a) and 9(b), respectively, as a function of solar elongation angle. Also presented in Figs. 9(a) and 9(b) are estimates of thermal noise and a solid model curve from [13].

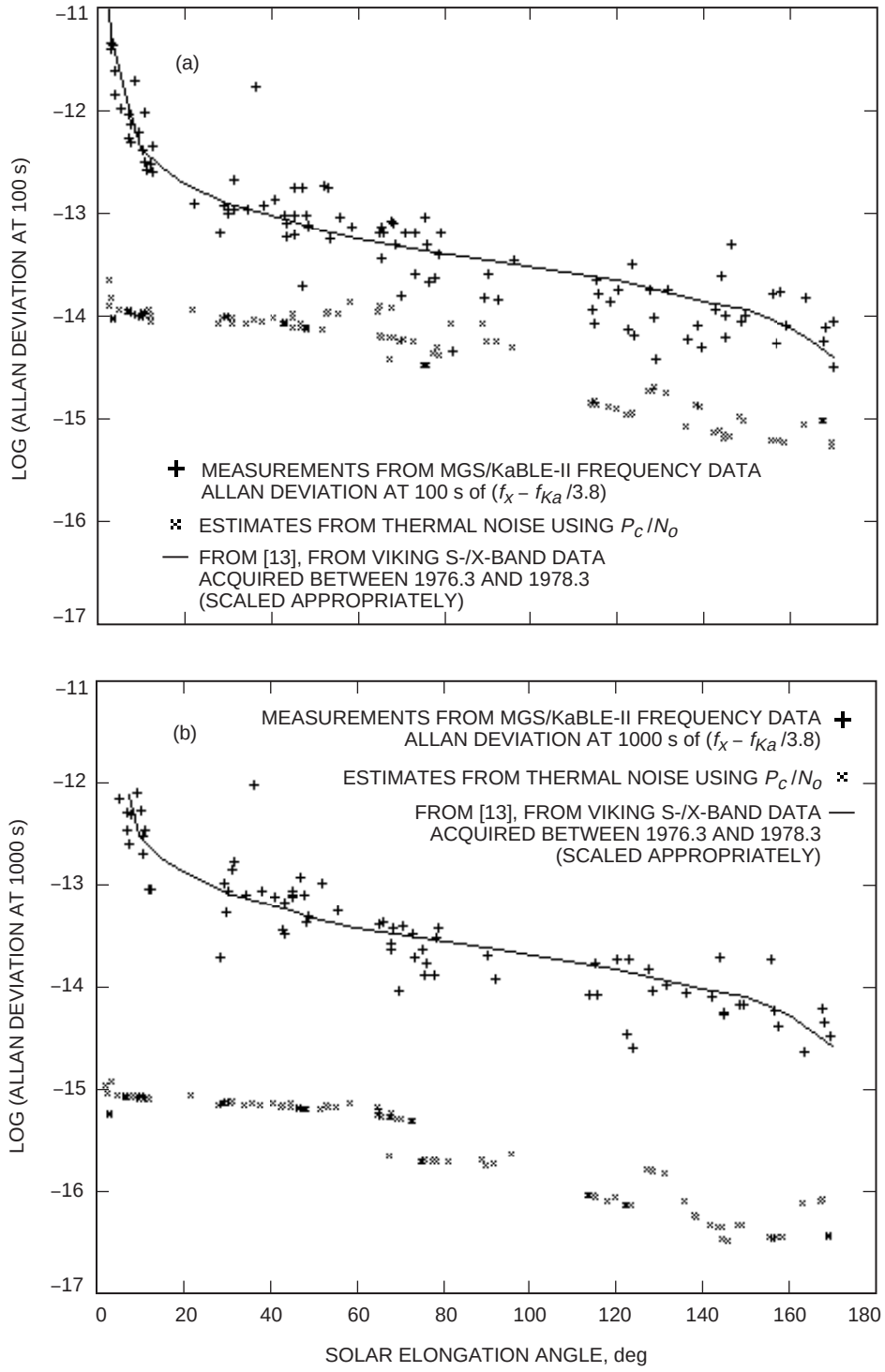

Fig. 9. Allan deviation versus solar elongation angle for the 1997–1998 2-year period of MGS link experiment data at (a) 100 s and (b) 1000 s.

A general trend is apparent that shows Allan deviation decreasing as solar elongation angle increases from near 2 deg to about 170 deg. This trend is consistent with the model curve derived from S-/X-band Viking data acquired between 1976 and 1978 [13]. The expected thermal noise contributions to the Allan deviations lie well below the observed values as shown. The majority of the 1000-s Allan deviations in Fig. 9(b) clustered at high solar elongation angles (above 160 deg) are in good agreement with a predicted Allan deviation of 6×10^{-15} for the anti-solar direction at X-band [13]. The Viking S-/X-band data acquisition and MGS X-/Ka-band data acquisition periods both occurred at approximately comparable durations and at about the same portions of the solar cycles near solar minimum.

VI. Conclusion

Scintillation and spectral broadening results at small SEP angles were presented for both X-band and Ka-band from the MGS 1998 solar conjunction experiment. These results were consistent with expected levels. The measured Allan deviation of the X-/Ka-band frequency difference and its signature with solar elongation angle were shown to be consistent with expected levels due to solar plasma. These data can be useful for current and future spacecraft projects to use for planning solar conjunction activities.

Acknowledgments

We would like to thank Richard Woo and John Armstrong for their invaluable support in providing guidance and encouragement during this endeavor. We would also like to thank J. Layland, J. Border, and H. Cooper of JPL, and W. Adams and A. McMechen of Lockheed-Martin Astronautics Co. for their technical expertise; P. Richter for his thorough review of the article; the DSS-13 station personnel for conducting the experiments; L. Teitelbaum and P. Wolken for scheduling support; and T. Priest and the Radio Science Support Team for their assistance and for making the BVR X-band data available.

References

[1] D. Morabito, S. Butman, and S. Shambayati, "The Mars Global Surveyor Ka-Band Link Experiment (MGS/KaBLE-II)," *The Telecommunications and Mission Operations Progress Report 42-137, January–March 1999*, Jet Propulsion Laboratory, Pasadena, California, pp. 1–41, May 15, 1999. http://tmo.jpl.nasa.gov/tmo/progress_report/42-137/137D.pdf

[2] S. Butman, D. D. Morabito, A. Mittskus, J. Border, J. Berner, C. Whetsel, M. Gatti, C. Foster, V. Vilnrotter, H. Cooper, A. Del Castillo, A. Kwok, J. Weese, M. Speranza, R. David, W. Adams, A. McMechen, C. Goodson, G. Bury, and D. Reece, "The Mars Global Surveyor Ka-Band Link Experiment (MGS/KaBLE-II)," *Proceedings of the 3rd Ka-Band Utilization Conference*, Sorrento, Italy, November 1997.

[3] D. Morabito, S. Butman, and S. Shambayati, "Recent Results from the Mars Global Surveyor Ka-band Link Experiment (MGS/KaBLE-II)," *Proceedings of the 4th Ka-Band Utilization Conference*, Venice, Italy, November 1998.

[4] D. Morabito, S. Butman, and S. Shambayati, "Mars Global Surveyor Ka-Band Frequency Data Analysis," *Proceedings of the 5th Ka-Band Utilization Conference*, Taormina, Italy, October 1999.

[5] Y. Feria, M. Belongie, T. McPheeters, and H. Tan, "Solar Scintillation Effects on Telecommunication Links at Ka-Band and X-Band," *The Telecommunications and Data Acquisition Progress Report 42-129, January–March 1997*, Jet Propulsion Laboratory, Pasadena, California, pp. 1–11, May 15, 1997.
http://tmo.jpl.nasa.gov/tmo/progress_report/42-129/129A.pdf

[6] D. H. Brown, W. J. Hurd, V. A. Vilnrotter, and J. D. Wiggins, "Advanced Receiver Tracking of Voyager 2 Near Solar Conjunction," *The Telecommunications and Data Acquisition Progress Report 42-93, January–March 1988*, Jet Propulsion Laboratory, Pasadena, California, pp. 75–79, May 15, 1988.
http://tmo.jpl.nasa.gov/tmo/progress_report/42-93/93G.PDF

[7] R. S. Bokulic and W. V. Moore, "Near Earth Asteroid Rendezvous (NEAR) Spacecraft Solar Conjunction Experiment," *Journal of Spacecraft and Rockets*, vol. 36, no. 1, pp. 87–91, January–February 1999.

[8] R. Woo and J. W. Armstrong, "Observations of Large-Scale Structure in the Inner Heliosphere with Doppler Scintillation Measurements," *Solar Wind*, eds. E. Marsch and R. Schwenn, Oxford: Pergamon Press, pp. 319–322, 1992.

[9] R. Woo, "Measurements of the Solar Wind Using Spacecraft Radio Scattering Observations, *Study of Traveling Interplanetary Phenomena*, Dordrecht-Holland: D. Reidel Publishing Company, pp. 81–100, 1977.

[10] T. A. Rebold, T. K. Peng, and S. D. Slobin, "X-Band Noise Temperature Near the Sun at a 34-Meter High Efficiency Antenna," *The Telecommunications and Data Acquisition Progress Report 42-93, January–March 1988*, Jet Propulsion Laboratory, Pasadena, California, pp. 247–256, May 15, 1988.
http://tmo.jpl.nasa.gov/tmo/progress_report/42-93/93V.PDF

[11] R. Woo and J. W. Armstrong, "Spacecraft Radio Scattering Observations of the Power Spectrum of Electron Density Fluctuations in the Solar Wind," *Journal of Geophysical Research*, vol. 84, no. A12, pp. 7288–7296, December 1, 1979.

[12] D. Morabito and S. W. Asmar, "Radio-Science Performance Analysis Software," *The Telecommunications and Data Acquisition Progress Report 42-120, October–December 1994*, Jet Propulsion Laboratory, Pasadena, California, pp. 121–152, February 15, 1995.
http://tmo.jpl.nasa.gov/tmo/progress_report/42-120/120B.PDF

[13] J. W. Armstrong, R. Woo, and F. B. Estabrook, "Interplanetary Phase Scintillation and the Search for Very Low Frequency Gravitational Radiation," *The Astrophysical Journal*, vol. 230, pp. 570–574, June 1, 1979.